The Astrophysical Journal, 641:1010–1017, 2006 April 20

THE GIANT X-RAY FLARE OF GRB 050502B: EVIDENCE FOR LATE-TIME INTERNAL ENGINE ACTIVITY

A. D. Falcone,[1] D. N. Burrows,[1] D. Lazzati,[2] S. Campana,[3] S. Kobayashi,[1,4] B. Zhang,[5] P. Mészáros,[1,6] K. L. Page,[7] J. A. Kennea,[1] P. Romano,[3] C. Pagani,[1,3] L. Angelini,[8,9] A. P. Beardmore,[7] M. Capalbi,[10] G. Chincarini,[3,11] G. Cusumano,[12] P. Giommi,[10] M. R. Goad,[7] O. Godet,[7] D. Grupe,[1] J. E. Hill,[1,8] V. La Parola,[12] V. Mangano,[12] A. Moretti,[3] J. A. Nousek,[1] P. T. O'Brien,[7] J. P. Osborne,[7] M. Perri,[10] G. Tagliaferri,[3] A. A. Wells,[13] and N. Gehrels[8]

Received 2005 August 30; accepted 2005 December 22

ABSTRACT

Until recently, X-ray flares during the afterglow of gamma-ray bursts (GRBs) were a rarely detected phenomenon; thus, their nature is unclear. During the afterglow of GRB 050502B, the largest X-ray flare ever recorded rose rapidly above the afterglow light curve detected by the *Swift* X-Ray Telescope. The peak flux of the flare was >500 times that of the underlying afterglow, and it occurred >12 minutes after the nominal prompt burst emission. The fluence of this X-ray flare, $(1.0 \pm 0.05) \times 10^{-6}$ ergs cm^{-2} in the 0.2–10.0 keV energy band, exceeded the fluence of the nominal prompt burst. The spectra during the flare were significantly harder than those measured before and after the flare. Later in time, there were additional flux increases detected above the underlying afterglow, as well as a break in the afterglow light curve. All evidence presented below, including spectral and, particularly, timing information during and around the giant flare, suggests that this giant flare was the result of internal dissipation of energy due to late central engine activity, rather than an afterglow-related effect. We also find that the data are consistent with a second central engine activity episode, in which the ejecta is moving slower than that of the initial episode, causing the giant flare and then proceeding to overtake and refresh the afterglow shock, thus causing additional activity at even later times in the light curve.

Subject headings: gamma rays: bursts — X-rays: bursts

1. INTRODUCTION

Since its launch on 2004 November 20, *Swift* (Gehrels et al. 2004) has provided detailed measurements of numerous GRBs and their afterglows with unprecedented reaction times. Of the 57 bursts detected by the Burst Alert Telescope (BAT; Barthelmy et al. 2004) as of 2005 August 3, 43 were observed by the narrow-field instruments in less than 200 ks (typical reaction time was much less, but occasionally BAT detected a burst that was observationally constrained). The narrow-field instruments include the X-Ray Telescope (XRT; Burrows et al. 2005a) and the Ultraviolet/Optical Telescope (UVOT; Roming et al. 2005). Of these 43 observations, 42 afterglows were detected by the XRT, and 30 of them received prompt (<300 s) observations with the pointed instruments. By detecting burst afterglows promptly and with high sensitivity, the properties of the early afterglow and extended prompt emission can be studied in detail for the first time. This also facilitates studies of the transition between the prompt emission and the afterglow.

While there are still many unknown factors related to the mechanisms that produce GRB emission, the most commonly accepted model is that of a relativistically expanding fireball with associated internal and external shocks (Mészáros & Rees 1997). In this model, internal shocks produce the prompt GRB emission. Observationally, this emission typically has a timescale of ~30 s for long bursts and ~0.3 s for short bursts (Meegan et al. 1996). The expanding fireball then shocks the ambient material to produce a broadband afterglow that decays quickly (typically as $\sim t^{-\alpha}$). When the Doppler boosting angle of this decelerating fireball exceeds the opening angle of the jet into which it is expanding, then a steepening of the light curve (jet break) is also predicted (Rhoads 1999). For a description of the theoretical models of GRB emission and associated observational properties, see Mészáros (2002), Zhang & Mészáros (2004), Piran (2005), and van Paradijs et al. (2000).

Several authors have suggested reasons to expect continued activity from the internal engine of the GRB after the classical "prompt" emission time frame. Katz (1997) considered a model in which a magnetized disk around a central black hole could lead to continued energy release in the form of internal shocks. The parameters of this energy release would depend on the complex configuration of the magnetic field and the magnetic reconnection dynamics, but time periods as long as days for the delayed emission were predicted. King et al. (2005) have speculated that episodic accretion processes could explain continued internal engine activity. These authors expect that fragmentation and subsequent accretion during the collapse of a rapidly rotating stellar core could explain observations of extended prompt emission. In general, the dominant model of an expanding fireball with

[1] Department of Astronomy and Astrophysics, Pennsylvania State University, University Park, PA 16802; afalcone@astro.psu.edu.
[2] JILA, 440 UCB, University of Colorado, Boulder, CO 80309.
[3] INAF–Osservatorio Astronomico di Brera, Merate, Italy.
[4] Center for Gravitational Wave Physics, Pennsylvania State University, University Park, PA 16802.
[5] Department of Physics, University of Nevada, Las Vegas, NV 89154-4002.
[6] Department of Physics, Pennsylvania State University, University Park, PA 16802.
[7] Department of Physics and Astronomy, University of Leicester, Leicester, UK.
[8] NASA Goddard Space Flight Center, Greenbelt, MD 20771.
[9] Universities Space Research Association, Columbia, MD 21044.
[10] ASI Science Data Center, Frascati, Italy.
[11] Università degli studi di Milano-Bicocca, Dipartimento di Fisica, Milano, Italy.
[12] INAF–Istituto di Fisica Spazialee Fisica Cosmica sezione di Palermo, Palermo, Italy.
[13] Space Research Center, University of Leicester, Leicester, UK.

internal/external shocks (Mészáros & Rees 1997) allows for continued prompt emission, provided that the internal engine is capable of continuing the energy injection.

A few previous observations have included indications of flaring from GRBs after the nominal prompt emission phase. Watson et al. (2003) used *XMM-Newton* to detect line emission from GRB 030227 nearly 20 hr after the prompt burst. They inferred continued energy injection at this late time and concluded that a nearly simultaneous supernova and GRB event would require sporadic power output with a luminosity in excess of $\sim 5 \times 10^{46}$ ergs s^{-1}. Piro et al. (2005) used *BeppoSAX* to observe two GRBs with relatively small X-ray flares. The X-ray flare times for GRB 011121 and GRB 011211 were reported as $t = 240$ and 600 s, respectively. The spectral parameters of these two X-ray flares were consistent with afterglow parameters, and these flares were interpreted as the onset of the afterglow (Piro et al. 2005). Two other examples of flaring and/or late-timescale emission can be found in in't Zand et al. (2003) and Galli & Piro (2005). Although not a detection of late flares from a particular GRB, the work of Connaughton (2002), in which an ensemble of GRBs was analyzed, should also be mentioned. In this study, 400 long GRBs detected by the Burst and Transient Source Experiment (BATSE) were analyzed together in the form of a summed light curve above 20 keV. Significant emission was found at late times (at least to 1000 s). There are several possible explanations for this emission that do not require flares, but flares at various times are certainly one possible explanation.

More recently, Burrows et al. (2005b) provided the initial report that two bursts detected by *Swift* showed strong X-ray flares. The first of these, XRF 050406, was an X-ray flash with a short and relatively weak X-ray flare that peaked 213 s after the nominal prompt emission. Due to the fast rise/decay, the most natural explanation for this flare is continued internal engine activity at late times (i.e., delayed prompt emission). A detailed analysis of XRF 050406 is provided by Romano et al. (2006). GRB 050502B, the subject of this paper, was also reported on by Burrows et al. (2005b), since it had a dramatic X-ray flare that peaked 740 s after the nominal prompt emission. This paper will now explore this event in more detail.

GRB 050502B was detected by the *Swift* BAT at 09:25:40 UT on 2005 May 2 (Falcone et al. 2005). According to Cummings et al. (2005), the T90 duration for the prompt emission detected by BAT was 17.5 ± 0.2 s, and the burst had three individual peaks. The main hard peak had a 6 s duration, was well fit by a power law with photon index 1.6 ± 0.1, and had a 15–350 keV fluence of $(8.0 \pm 1.0) \times 10^{-7}$ ergs cm^{-2} (Cummings et al. 2005). The spacecraft slewed promptly, and observations with *Swift* XRT and *Swift* UVOT began 63 s after the BAT trigger time. Since the flux was initially low, the XRT image mode data did not produce an initial onboard centroid position; however, the first pass of data was analyzed on the ground, leading to an XRT position of R.A. $= 09^{\rm h}30^{\rm m}10\overset{\rm s}{.}1$, decl. $= +16^\circ 59^{\rm m}44\overset{''}{.}3$ (J2000), with a 90% containment uncertainty of $5''$ (Pagani et al. 2005). There was no counterpart found by UVOT, but ground-based optical observations reported by Cenko et al. (2005) revealed a fading afterglow at R.A. $= 09^{\rm h}30^{\rm m}10\overset{\rm s}{.}02$, decl. $= +16^\circ 59^{\rm m}48\overset{\rm s}{.}07$ (J2000), which is within $4''$ of the reported XRT position. Following the initial low-flux detection by XRT, continued monitoring revealed increased flux that turned out to be the largest X-ray flare ever detected during a GRB afterglow. This giant X-ray flare was not accompanied by any detected emission in the BAT energy band.

2. OBSERVATIONS

In this paper, we are reporting observations and analysis with the XRT data set. The XRT began taking data on this burst within 63 s after the BAT prompt emission trigger. After the initial data taken in image mode, the spacecraft executed its usual sequence of modes and began taking windowed timing (WT) mode data. Since the rate was initially low, the telescope then switched into photon counting (PC) mode. Throughout the initial data segment, there was significant mode switching between PC mode and WT mode. The initial data segment (data taken after the autonomous slew) contained 57.8 ks of data after screening. Following this autonomous slew, follow-up observations were scheduled on GRB 050502B, which resulted in a total of 178 ks of data taken over a time period ranging from 63 s to 10.6 days after the BAT trigger.

3. ANALYSIS

Data were reduced using the latest HEAsoft tools (ver. 6.0), including *Swift* software version 2.0, and the latest response (ver. 7.0) and ancillary response files (created using `xrtmkarf`) available in CALDB at the time of analysis. Data were screened with standard parameters. Data were also screened to eliminate time periods when the CCD temperature was warmer than -50° C. When analyzing WT data, only grades 0–2 were included, and when using PC mode data, only grades 0–12 were included. Source and background regions were specified independently for each data segment using the image from all data in that segment. For PC mode data, the source region was a 30 pixel radius circle during the initial data segment when the source was very bright, and it was a 15 pixel radius circle for all subsequent data segments. The background region was chosen in a source-free region of the image and was a circle with twice the radius of the source region in each data segment. Background for WT mode data was found to be negligible. The light curves were binned such that all bins contained >8 counts after background subtraction (actually, most bins had hundreds of counts).

Spectral models were fit to data using Xspec version 12.2.0. Spectra were fit in the 0.2–5.5 keV energy range. The energy range above 5.5 keV was excluded, since some of the time regions before and after the giant flare had almost no counts above this energy. In the interests of maintaining consistency in the analysis, a common upper bound (5.5 keV) was chosen for the energy range used in the fit. A systematic error of 3% was assigned throughout the energy range due to uncertainties in the response of the instrument. The response below 0.6 keV is more uncertain, since calibration is more difficult in this energy range; thus, a systematic error of 5% is assumed in the range 0.2–0.6 keV. During fitting, χ^2 statistics were used when appropriate (always with >20 photons bin^{-1}). In the preflare time region when there were low counts ($\approx$60 counts), the *C*-statistic was used, and the spectral data were binned to 1 photon bin^{-1}, which is more appropriate for the *C*-statistic (Cash 1979; Nousek & Shue 1989).[14] In general, the *C*-statistic provides better parameter estimation when there are few or no background counts and when source counts are low, so it was used to estimate parameters during the fitting. Following the parameter estimation, χ^2 statistics were then applied to these parameter values as an extra consistency check.

During the preflare and flare time regions, mode switching led to collection of both PC mode data and WT mode data. When the count rate was high ($\gtrsim 0.5$ counts s^{-1}), WT mode data were used, rather than PC mode data, in order to avoid effects due to pile-up on the detector. This did not detract significantly from the data, since there was nearly equivalent WT and PC mode coverage throughout the time period before and during the flare when

[14] See also http://heasarc.gsfc.nasa.gov/xanadu/xspec.

the count rate was high. WT mode data are free of significant pile-up effects throughout the entire range of flux reported in this paper, since pile-up does not begin to effect WT mode data until 1 crab (Burrows et al. 2005a). The PC and WT mode light curves before and after the flare were compared to each other to be sure that the data points with little or no pile-up were consistent with each other.

4. RESULTS

4.1. *Light Curve*

The overall light curve for GRB 050502B is shown in Figure 1. Since the PC mode data were piled-up during the bright flare, the more reliable WT mode data were used for periods when the count rate was high ($\gtrsim 0.5$ counts s^{-1}). However, it is worth pointing out that the piled-up data (with a correction applied) and non-piled-up data in PC mode match the WT mode data during the flare; thus, there should be no systematic shift in a light curve that contains both types of data. The overall light curve has many features. There is an obvious underlying decay curve. Superimposed on this decay is a rapid and intense rate increase, beginning at 345 ± 30 s. For clarity, we refer to this large rate increase as the giant flare throughout the remainder of the text. There is also significant shorter timescale variability near the peak of the giant flare when viewed in the hard band (1.0–10.0 keV), as shown in Figure 2. Following the giant flare, the underlying decay continues at a decay rate consistent with the decay rate before the giant flare. After several hours ($>10^4$ s), two significant bumps in the X-ray emission occur consecutively. At an undetermined time during or after the bumps, the underlying decay becomes steeper.

The underlying decay before and after the giant flare can be fit by a single power law that decays as $\sim t^{-\alpha}$, where $\alpha = 0.8 \pm 0.2$ (the error bar is dominated by systematic variations associated with the choice of flare start and stop times), and t_0 is taken as the time of the prompt burst. As can be seen from Figure 3, fitting the preflare light-curve data and the postflare light-curve data independently does not significantly improve the fit. In this plot, the dotted lines represent fits to the preflare and postflare data independently of one another (resulting in decay curves $\sim t^{-1.0\pm0.3}$ and $\sim t^{-0.7\pm0.3}$, respectively), while the solid line represents a fit of all preflare and postflare data ($\sim t^{-0.8\pm0.2}$). The lines in Figure 3 lie on top of one another, within error, indicating that there is no evidence for a change in the underlying decay after the giant flare, relative to that before the giant flare. Aside from the flare itself, there is no evidence for any increase in the underlying decay flux relative to the preflare extrapolation of the decay (i.e., there is no evidence for afterglow shock reenergization near the time of the flare), but a factor of ~ 2 increase of the postflare flux relative to the preflare flux could be possible within the error bars of the data.

The giant flare begins to rise up above the underlying decay curve at 345 ± 30 s. It rises to a sharp peak at 743 ± 10 s, but this appears to be on top of a broader peak that extends from 640 ± 20 to 790 ± 20 s. There is significant time structure within the peak of the giant flare itself, particularly in the harder X-ray light curve (see Fig. 2). The rise and decay of the giant

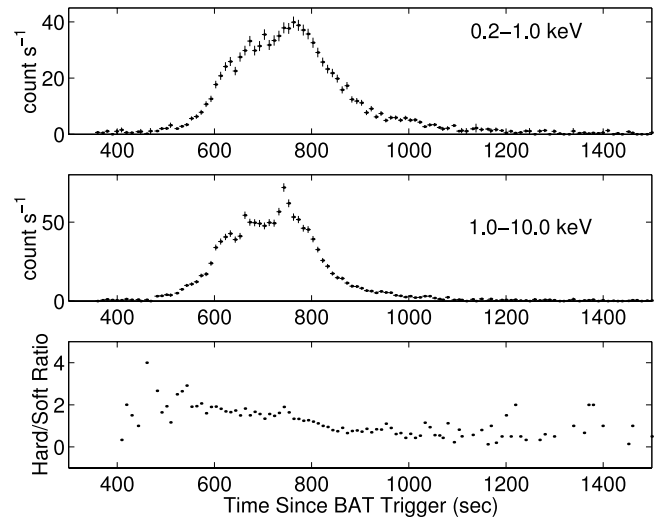

FIG. 2.—Hard/soft band ratio of GRB 050502B. Error bars are 1 σ statistical errors.

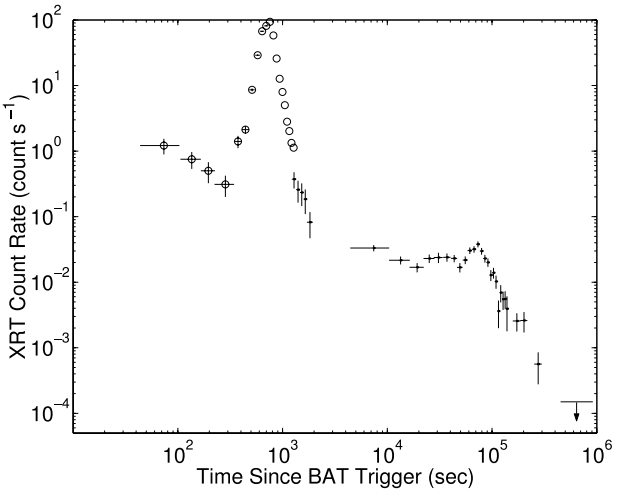

FIG. 1.—Overall 0.2–10 keV band light curve of GRB 050502B. Vertical error bars are 1 σ statistical errors. Horizontal error bars represent time bin size. Open circle points represent WT mode data, and dots represent PC mode data. The "giant flare" is the obvious >500 times rate increase at (345 ± 30) s. There is also some bumpiness and/or flattening evident in the light curve at $\gtrsim 10^4$ s, as well as an underlying decay below all of this activity. Last datum is 90% confidence level upper limit.

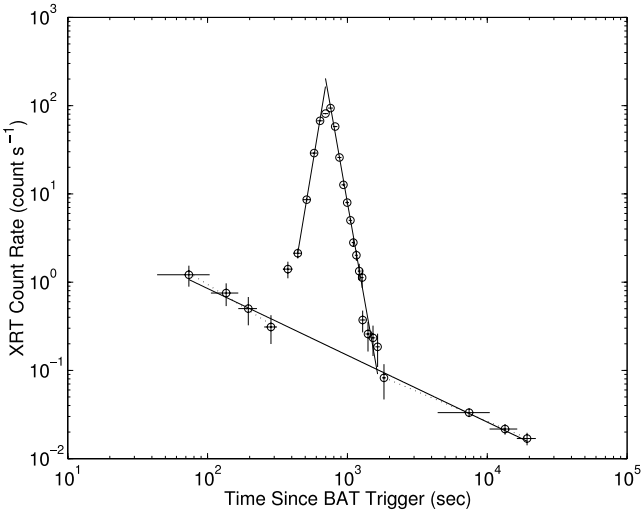

FIG. 3.—Flare and fit to underlying decay curve of GRB 050502B, in the 0.2–10 keV energy band. During the underlying decay, the solid line corresponds to a fit of all data points shown before and after the flare. The dotted lines, which are fits to the preflare and postflare data independently, do not deviate significantly from fitting all underlying data simultaneously. Vertical error bars are 1 σ statistical errors. Horizontal error bars represent the time bin size.

flare can both be fit by simple power laws below the broad peak. The flare rises rapidly as $\sim t^{9.5\pm2.1}$, and it decays rapidly as $\sim t^{-9.0\pm1.5}$. If the underlying power-law decay is subtracted from the giant flare data, then the rise is fit as $\sim t^{9.9\pm2.2}$, and the decay is fit as $\sim t^{-9.2\pm1.6}$. The fits were all done using flare data outside of the 150 s region defining the peak and assuming a time origin at the burst trigger time. Over the total 1360 s duration of the giant flare (837 s of good observation time), there were 23,352 excess photons (in excess of both background and underlying decay-curve extrapolation) collected in WT mode. If one assumes that the 30 s duration hard X-ray rise at the top of the giant flare is a subflare, then the significance of only this short variation is 6.4 σ, with 376 photons detected in excess of the giant flare broad peak.

Following the decay of the giant flare, the light curve continues to decay at the preflare decay rate until $\sim 10^4$ s. Starting after $(1.9 \pm 0.3) \times 10^4$ s, there are two consecutive broad bumps in the light curve, or possibly a flattening combined with a bump. The time frame for the first bump is estimated to be $(1.9 \pm 0.3) \times 10^4$ to $(4.9 \pm 0.3) \times 10^4$ s, and the time frame for the second bump is taken as $(4.9 \pm 0.3) \times 10^4$ to $(1.1 \pm 0.1) \times 10^5$ s. The large error bar on the last data point is dominated by our inability to deconvolve the decay of the second bump from the faster decay of the underlying light curve after the second bump. Given the time frames stated above, the signal-to-noise ratio (S/N) of the excess over the underlying decay curve for the first bump is 6.6 σ, and the S/N of the excess over the underlying decay for the second bump is 17 σ.

After the two late bumps (or possibly during the second bump), the slope of the light curve becomes steeper. The last detection on the light curve and the upper limit shown in Figure 1 are significantly below the power-law decay extrapolated from times prior to the late bumps. The 90% confidence level upper limit is a factor of 8 below the extrapolated curve. It is difficult to estimate the time at which the steepening begins or the exact slope, since we cannot be certain of the contribution of the second late bump relative to the underlying decay curve itself. If one fits the data above 1.1×10^5 s with a power-law decay, then the resulting decay index is $\alpha = 2.8 \pm 0.8$.

4.2. *Spectra*

4.2.1. *Hard/Soft Band Ratio*

The hard/soft band ratio, as well as the light curves in the respective bands, are shown in Figure 2. Three things are clear from this plot. First, the hard/soft band ratio increases during the flare and subsequently decays as the flare decays. We note the similarity to the spectral evolution of prompt GRB emission. Second, the hard band shows significant short-timescale variability, particularly near the peak of the giant flare (as discussed previously). Third, the hard band begins to decay more quickly than the soft band. Furthermore, the soft band has a shallower decay slope, relative to the slope of the flare rise. It is clear from this plot that the hardness ratio increases at the onset of the flare, independent of any modeling, since this is merely a band ratio plot with no model dependence.

4.2.2. *Spectral Fits*

The spectra throughout the X-ray flaring and the underlying decay can be adequately fit by a simple power law with absorption, which looks like

$$f = C\left(e^{-N_{\rm H}\sigma(E)}\right)\left(\frac{E}{1\ {\rm keV}}\right)^{-\eta}, \qquad (1)$$

where $N_{\rm H}$ is the neutral hydrogen column density in units of atoms cm^{-2}, $\sigma(E)$ is the energy-dependent photoelectric absorption cross section (Morrison and McCammon 1983), η is the spectral photon index (note that η was chosen rather than the usual Γ or α, to avoid confusion with the bulk Lorentz factor or with the power-law temporal decay index), and C is the normalization constant in units of photons cm^{-2} s^{-1} keV^{-1}. These fits lead to χ^2/dof values that range from 0.67 to 1.21, as a function of the time used in the fit, except during the giant flare at which time the χ^2/dof reaches a value of 1.44 (328 dof) at the peak of the flare. These fits lead to $N_{\rm H}$ values that rise significantly during the onset of the flare and then decay after the flare; but outside of the giant flare time region, the $N_{\rm H}$ values are reasonable. Other models were explored and found to produce as good or superior fits, without the need for an apparent increase in the column density.

In general, the prompt emission from GRBs can be more realistically fit with Band functions (Band et al. 1993), rather than simple power laws. Since the giant X-ray flare could be due to the same mechanisms that produce the nominal prompt emission, it is reasonable to try to fit Band function or Band function–like models to the time periods when the flare was dominating the observed emission. For the soft X-ray observations being analyzed here, nearly all of the photons are below any reasonable Band function cutoff energy. As a result, spectral fits with a power law multiplied with an exponential cutoff are nearly equivalent to fits with a Band function, and these fits require fewer parameters and lead to better convergence on photon-limited data. We have explored this by fitting several time periods during and around the giant flare with both absorbed Band functions and absorbed cutoff power laws. We find that both of these models fit the flaring-time regions significantly better than the simple power-law models, whereas the absorbed power-law models fit better during time periods when the flare was not dominating the emission. The Band function models and the power laws with exponential cutoffs fit equally well during the flare, and the exponential cutoffs provide better convergence due to the reduced number of parameters to be fit. At the peak of the flare, the cutoff power law fit the data with a χ^2/dof of 1.21. The cutoff power law was compared to the simple power law using the F-test, resulting in an F-test probability of $\approx 3 \times 10^{-14}$, supporting the improvement of the fit using the cutoff power law rather than the simple power law. When this fact is coupled with the increasing column density values obtained using the simple power law and the prompt-emission-like timing properties of the giant flare, it is clear that the cutoff power law is more applicable to the flaring-time region. So for the remainder of the analysis, we have used the absorbed power law with exponential cutoff to fit time periods during the giant X-ray flare, and we have used an absorbed simple power law to fit all other time periods.

The absorbed power law with exponential cutoff has the following form,

$$f = C\left(e^{-N_{\rm H}\sigma(E)}\right)\left(\frac{E}{1\ {\rm keV}}\right)^{-\eta}\left(e^{E/E_{\rm cut}}\right), \qquad (2)$$

where $N_{\rm H}$ is the neutral hydrogen column density (as before), η is the spectral photon index, $E_{\rm cut}$ is the characteristic cutoff energy in units of kilo–electron volts, and C is the normalization constant in units of photons cm^{-2} s^{-1} keV^{-1}. Since some models predict column density variations, we left $N_{\rm H}$ free to vary throughout the fitting procedure, but we did set the lower bound of the $N_{\rm H}$ to the measured Galactic value (Dickey & Lockman 1990).

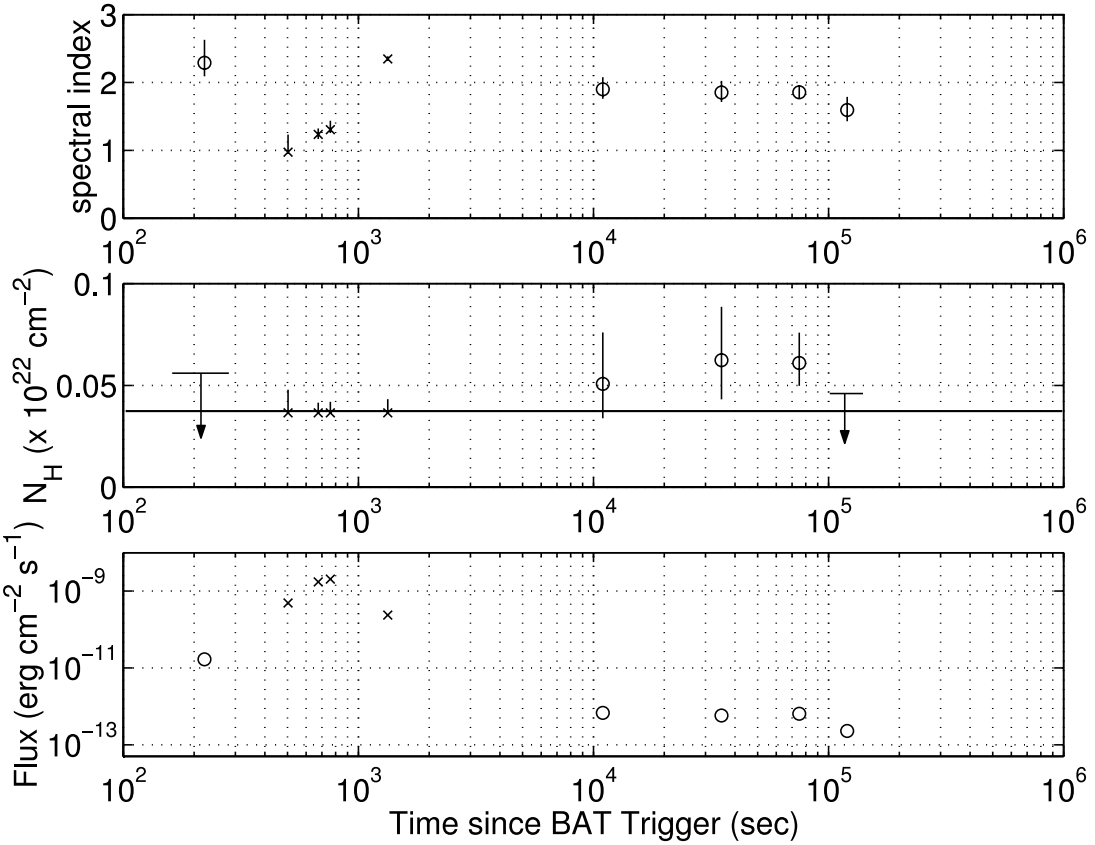

FIG. 4.—Spectral parameters of GRB 050502B. Open circle data points (during nonflare time periods) represent parameter values fit using an absorbed simple power-law model. Data points denoted with crosses (during giant flare) represent parameter values fit using an absorbed power law with an exponential cutoff. The top panel shows an obvious hardening during the giant flare. During the flare, the value for $E_{\rm cut}$ was free, but it remained at 2.5 ± 0.2 keV, except during the transition from the flare decay to the underlying light-curve-dominated emission. $N_{\rm H}$, shown in the middle panel, was a free parameter, but it was required to be above the Galactic value (Dickey & Lockman 1990), which is shown as a solid line across the plot; this is the reason for the uneven error bars during the flare. Error bars are 1 σ statistical errors, assuming two parameters of interest. Upper limits are 90% confidence level.

The results of applying the absorbed power law with an exponential cutoff model to the flare and an absorbed power law to the nonflare time regions are shown in Figure 4. The value of $E_{\rm cut}$ is not plotted in Figure 4, since it was consistent with a constant value of 2.5 ± 0.2 keV during the flare, with one exception. During the final decay of the flare, $E_{\rm cut}$ was large enough (>170 keV) to make the cutoff power-law model effectively become a simple power-law model with characteristics similar to the underlying decay. There is significant variability of the soft X-ray spectral index during the giant flare, as can be seen in the top panel of Figure 4. The data prior to the giant flare appear to have spectral fits that are consistent with the spectral fits after the flare. During the giant flare, the spectrum hardens significantly; then, during the decay of the flare, it begins to soften back to a value consistent with the spectrum during the underlying light curve before and after the flare. By the time the underlying emission is dominating the light curve again, the spectrum appears to have become soft again, as it was before the flare. This softening during the decay of the flare is caused by the faster decay of the hard emission, as seen in Figure 2. There is also a weak indication of some gradual hardening of the spectrum as the underlying flux fades. All of the fit parameters displayed in Figure 4 fit the data well; the χ^2/dof ranged from 0.62 to 1.21. A sample spectral fit, calculated during the rising edge of the giant flare, is shown in Figure 5.

5. ENERGY OF THE GIANT X-RAY FLARE

During the time period of the giant X-ray flare, the total fluence in the 0.2–10.0 keV band was $(1.2 \pm 0.05) \times 10^{-6}$ ergs cm^{-2}. After subtracting the underlying light-curve data, the total fluence from the flare only is calculated to be $(1.0 \pm 0.05) \times 10^{-6}$ ergs cm^{-2}, in the same energy band. This fluence actually exceeds the fluence measured during the prompt emission phase by BAT in higher energy bands, which was $(8.0 \pm 1.0) \times 10^{-7}$ ergs cm^{-2} in the 15–350 keV band (Cummings et al. 2005).

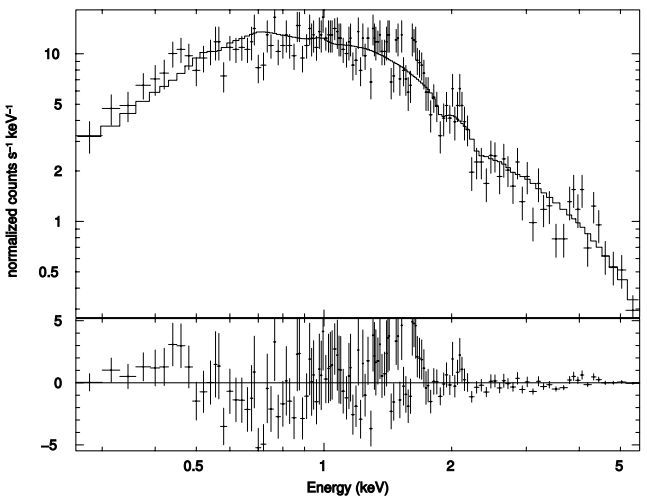

FIG. 5.—Example of a spectral fit using the absorbed power-law model with an exponential cutoff. This fit used data during the rising edge of the giant X-ray flare. Residuals of the fit are shown in the bottom plot.

6. DISCUSSION

The fast variability timescales and the magnitude of the giant flare seem to favor an internal engine origin for the emission, as opposed to a mechanism associated with the afterglow. Before looking at the supporting evidence for internal engine origin, let us first consider some afterglow-related possibilities. Discontinuities in the jet environment cannot explain the fast rise, $\sim t^{9.5\pm2.1}$, and small $\delta t_{\rm rise}/t_{\rm peak} \sim 0.5$. Rise and decay times associated with the forward shock encountering discontinuities are expected to be much longer than the times for these observations (Ioka et al. 2005). Explanations for the giant flare involving a refreshed shock are also ruled out, since there is no evidence for a shift in the preflare versus postflare light curve that would indicate energy injection into the external shock. The preflare and postflare light curves can be extrapolated to one another with near-perfect overlap, indicating a continuous underlying afterglow extending from times well before the X-ray flare. The giant flare is also steeper than one would expect if it was due to refreshing of the shock. Explanations involving a reverse shock, and associated synchrotron and synchrotron self-Compton emission (Kobayashi et al. 2005; Zhang et al. 2006), can be marginally accommodated by $\delta t/t \approx 1$; however, the large relative increase (factor of $\sim$500 times) of the giant flare over the afterglow and the faster variability at the peak of the flare makes these models less tenable in this case (Kobayashi et al. 2005; Zhang et al. 2006). Furthermore, the synchrotron emission from a reverse shock model for this flare would require associated strong UV-optical flaring, which was not observed.

Interpreting this giant flare as the start of the afterglow phase (Piro et al. 2005) is also inconsistent with the data. It is apparent from the light curve and from the spectral index before and after the flare that the afterglow began before the start of the X-ray flare. The temporal power-law decay index just before the flare matches the index just after the flare, as does the spectral index. This favors independent mechanisms for production of the X-ray flare photons and the underlying afterglow photons.

Spectroscopically, the afterglow and giant flare show interesting features. Initially, we fit the whole evolution with an absorbed power-law model, i.e., that expected from an afterglow created by a blast wave shock front. We found that this model provided a marginally good description of the data only if the absorbing column was left free to vary. The resulting evolution tracks the flux evolution: the apparent $N_{\rm H}$ is initially low, increases abruptly when the flare begins, and then progressively decreases back to a value consistent with the preflare $N_{\rm H}$. Lazzati & Perna (2002, 2003) predicted and discussed evolution of an X-ray absorbing column due to the progressive photoionization of the absorbing ions by the burst and afterglow UV and X-ray radiation. The recombination timescale for any reasonable density of the ambient medium is longer than the observed times, and therefore the X-ray column is expected to decrease in time. Such behavior has been observed in a few GRBs with *BeppoSAX* (Lazzati & Perna 2002; Frontera et al. 2004). For the giant flare from GRB 050502B, an *increase* of the absorbing column is required at the onset of the flare, if an absorbed power law is assumed, and even this does not provide a particularly good fit. This is hard to interpret in terms of photoionization of the absorbing medium. Small increases of the absorbing column can be accounted for if the external medium is clumped, since the surface of the emitting fireball is increasing in time due to its deceleration. However, an increase of the column by a factor of $\sim$10 seems unlikely, since the clumps will affect only a small portion of the visible fireball.

This apparently unrealistic $N_{\rm H}$ increase, combined with the hypothesis that the giant flare was caused by the same mechanism as the nominal prompt emission (supported by the fast timing structure of the giant flare), motivated the fits to the data using a model that included an exponential cutoff. This resulted in better fits to these data, and it resulted in more self-consistent spectral parameters. In particular, the $N_{\rm H}$ no longer appeared to increase dramatically at the onset of the flare and was consistent with the Galactic value of 3.65×10^{20} atoms cm^{-2} (Dickey & Lockman 1990). The data do allow for the possibility that the $N_{\rm H}$ was slightly higher after the flare, but it is certainly not required within the statistical and systematic errors that are present in the fitting procedure. If the $N_{\rm H}$ was slightly higher before and after the flare, with a decrease to Galactic values during the flare, this could be explained by photoionization; however, the final upper limit data point does not support this interpretation. The simplest interpretation is that the $N_{\rm H}$ was constant at approximately the Galactic value, with only slight fluctuations due to statistical and systematic errors.

As discussed above, we considered the possibility that the giant flare was due to late-time internal shocks related to a late rebrightening of the inner engine. In this case, the flare spectrum should be described with a Band function or an exponential cutoff power law rather than a simple power law, as is usually observed for typical prompt GRB emission. Allowing for this extra degree of freedom, we find that a good fit can be obtained without the previously described dramatic evolution of the absorbing column. The unabsorbed spectrum hardens sensibly during the flare, and the spectral shape is similar to that observed in X-ray flashes. Following the giant flare, the spectral index returns to a value consistent with the softer afterglow spectrum observed before the flare. This spectral evolution adds to the evidence discussed above for an internal shock origin of the giant flare.

The two bumps at $\gtrsim 10^4$ s can be interpreted in a variety of ways. Observationally, they are not well constrained. They appear to be two late and broad flares with a subsequent increase in the afterglow decay rate (i.e., steepening of the light curve). This increase in the decay rate could begin any time after the peak of the second bump; thus, the interpretation of the timescales is difficult. However, it is clear that there are two significant rate increases on top of the afterglow decay. These two bumps could be continued internal engine activity, but the longer timescales and the spectral parameters do not require this interpretation. The bumps could be caused by density fluctuations in the external medium through which the afterglow shock is propagating. The bumps could also be due to energy injection into the afterglow shock front and/or an associated reverse shock. This energy could come from material emitted from the internal engine that gets emitted at a later time than the initial prompt emission or that gets emitted with a slower speed.

The data show no evidence of rebrightening immediately after the giant flare. Evidence for rebrightening does not present itself until $\gtrsim 10^4$ s. If the giant flare is due to a delayed ejection episode from the central engine, this will eventually have to catch-up with the initially emitted ejecta, and a brightening above the underlying afterglow by about a factor of 2 would be expected. The time at which the catch-up is observed depends on the Lorentz factors of the two ejecta, on the energetics, and on the external medium properties. In Figure 6, we explore the feasibility of this model using a contour plot of the observed time at which the reenergization would be expected to take place as a function of Γ_1 and Γ_2, the Lorentz factors of the material associated with the initial ejection episode and of the delayed one, respectively. A total energy of 10^{52} ergs for the initial ejection

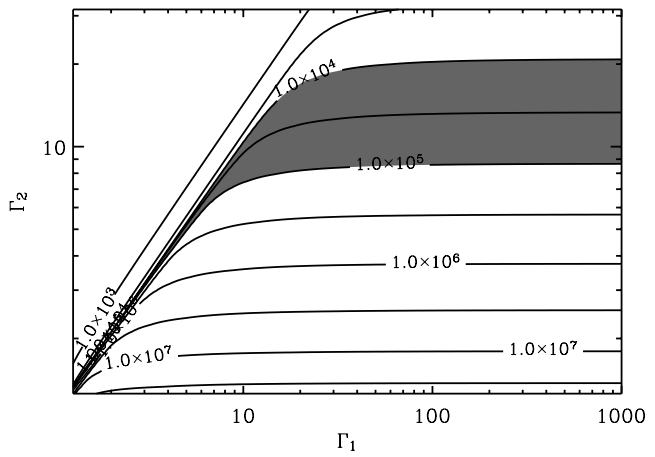

FIG. 6.—Contour plot of the observed time of reenergization (in seconds) due to the collision between the first ejecta, which has initial Lorentz factor Γ_1 and hypothetically produces the initial prompt emission, with the delayed ejecta, which has Lorentz factor Γ_2 and hypothetically produces the giant X-ray flare emission. The shaded region shows the area consistent with the two late-time bumps that may be caused by this collision.

episode is assumed (relevant if the GRB lies at $z \sim 1$ and the internal shock has a radiative efficiency of $\sim$0.3). A uniform external medium with density $n = 10$ cm^{-3} is also assumed (assuming $n = 1$ cm^{-3} has only a marginal effect and does not impact conclusions). The gray shaded area shows the region $10^4 \leq t_{\rm coll} \leq 10^5$ s, where the late-time bumps of unknown origin are observed. *If* one assumes that this model is correct, the plot shows two important things: (1) the second flow of ejecta started slower than the first one, and (2) it had a Lorentz factor $\Gamma_2 \lesssim 20$.

In the simplest version of synchrotron internal shocks, where the logarithmic dispersion of the Lorentz factor does not depend on the average Γ of the flow, the peak frequency of the spectrum is inversely proportional to the Lorentz factor (Ghisellini et al. 2000). In the model that attempts to explain the giant flare and the late-time flux increase described in the paragraph above, we see the opposite behavior: the higher the Lorentz factor, the higher the peak frequency (since the larger Γ_1 is associated with the BAT-detected prompt emission, and the smaller Γ_2 is associated with the giant X-ray flare). A way out of this inconsistency is to assume that the logarithmic dispersion of Lorentz factor is smaller when the average Lorentz factor is smaller. This would produce smaller peak frequencies for smaller Lorentz factors. Since the spectral properties of the flare are similar to X-ray flash spectra, it is tantalizing to infer that X-ray flashes might share this property. Alternatively, one could attempt to explain the bumps at $>10^4$ s as being due to even later internal engine activity. More detailed studies to model the energy budget and the timing of sporadic and late internal engine emission will be necessary to discriminate between these two competing possibilities for the bumps in the light curve at times $>10^4$ s.

If one assumes that the giant flare was due to a process similar to the initial prompt emission, the peak energy should be roughly proportional to $L_{\rm iso}^{1/2}$, with significant spread around the expectation values, as shown for a sample of bursts by Ghirlanda et al. (2005). Qualitatively, this is consistent with the data; the initial prompt emission relative to the giant flare emission peak luminosity is about 2 orders of magnitude higher, and the peak energy decreases from 80 to 3 keV. The downward shift of peak energy is possibly a bit more than expected by the simple scaling with $L_{\rm iso}^{1/2}$, which could in principle be influenced by the relative Lorentz factors of the two ejection episodes. However, the systematic errors due to the differing energy ranges of the initial prompt emission and the giant flare, as well as the measured spread in the peak energy to luminosity relationship, allow for order-of-magnitude variation.

In addition to flaring, a steepening was observed in the light curve beyond $\sim 1.1 \times 10^5$ s. One obvious interpretation of this is that a jet break has been observed. A jet break is a steepening of the light-curve decay that occurs when the relativistic beaming angle, which is increasing as the fireball Doppler factor is decreasing, begins to exceed the physical opening angle of the jet (Rhoads 1999). One can calculate the jet opening angle as a function of the jet break time, assuming a fireball model expanding into a constant density interstellar medium. This leads to $\theta_0 = 7.^\circ 8 t_5^{3/8} E_{52}^{-1/8} n_{\rm ism}^{1/8} [(1+z)/2]^{-3/8}$, where t_5 is the jet break time in units of 10^5 s, E_{52} is the isotropic energy in units of 10^{52} ergs, $n_{\rm ism}$ is the interstellar medium density in units of cm^{-3}, and z is the redshift. Assuming typical parameters and a jet break time of $\sim 1.1 \times 10^5$ s leads to an opening angle of $\sim 8.^\circ 1$, which is within the typical range of bursts observed and studied with known redshifts (Bloom et al. 2003). Alternatively, this steeper slope could be interpreted as the end of a period of continuous energy injection that was feeding the afterglow shock, thus creating a shallower decay slope followed by a steepening when the continuous energy injection phase ends. However, the work of Zhang et al. (2006) suggests that this type of break would lead to a steepening of the light-curve decay index to $\sim$1.2, whereas the data in this case suggest a steepening to a decay index of $\approx 2.8 \pm 0.8$, which is more indicative of a jet break. While the model in which the break is caused by an end to continuous energy injection is not ruled out here, it seems that a jet break is the more likely explanation for the steepening in the light curve after $\sim 1.1 \times 10^5$ s. The data from this burst, as well as other flaring bursts found in the *Swift* XRT data, should allow much more rigorous studies of the various models and their predicted temporal and spectral parameters.

It is also possible, within the error bars of the temporal power-law decay indices, that the underlying afterglow decay index was steeper ($\alpha \sim 1.0$) throughout the whole curve and that the entire light curve, between the start of the giant flare and the final data point on Figure 1, was due to internal engine flaring and energy injection. This scenario seems less likely, since the features of the light curve and spectra before and after the giant flare match each other well and since it *requires* even later internal engine activity. This scenario is mentioned, since it is possible within the error bars of the data; however, the data certainly do not require or suggest this interpretation.

7. CONCLUSIONS

The complex light curve of GRB 050502B has many interesting features. The most interesting of these is a giant flare with a fast rise/decay that began at 345 ± 30 s, well after the nominal 17.5 ± 0.2 s prompt GRB phase. This is the largest X-ray flare ever detected after the apparent cessation of prompt emission. After compiling all of the evidence, we come to the conclusion that the simplest explanation for this flare is continued activity in the internal engine of the GRB, not associated with the afterglow external shock. This evidence includes:

1. The temporal decay index before and after the flare is identical, within error, indicating that the afterglow had already begun before the flare.
2. The rise time and decay time of the flare are very fast; thus, the flare is difficult (although not impossible) to explain with mechanisms associated with the external shock.

3. There is even faster time structure near the peak of the flare in the band above 1 keV.

4. The spectra during the giant flare are represented better by a Band function or cutoff power-law model, rather than a simple power law.

5. The spectra before and after the flare are consistent with an afterglow that has already begun before the flare and continues with approximately the same spectral index after the flare, whereas the spectra during the flare are significantly harder.

6. Based on recent data there appear to be many other similar flares, although not as intense as this one, with even faster time profiles (suggesting extended internal engine activity) in up to $\sim\frac{1}{2}$ of the *Swift*-detected GRBs.

The two late bumps in the light curve (at $>10^4$ s) are not as well constrained, so conclusions are not as firm. They could be due to more internal engine activity, such as that which created the giant flare, or they could be due to another process associated with the afterglow shock. If one or both of these bumps is due to reenergization of the afterglow shock due to the same internal engine ejection episode that created the giant flare at $\sim$345 s, then this ejecta must have been emitted with a Lorentz factor $\Gamma_2 \lesssim 20$, and it must have been traveling slower than the primary ejecta that created the BAT-detected prompt emission. However, the limits on Γ_2 are obviously dependent on the presumption that the bumps at $>10^4$ s are due to reenergization of the afterglow shock by the same ejecta responsible for the giant flare. Although this presumption is consistent with the data, it is not the only possible explanation, as stated earlier. We can also conclude that there was a steepening of the light curve at some time during or after the late bumps (i.e., after $\sim 5 \times 10^4$ s). This steepening could have been a jet break, or it could have been the end of a phase of continuous energy injection into the afterglow shock front.

This GRB, and the associated X-ray flare, can be most easily explained within the framework of the standard GRB fireball model (Mészáros & Rees 1997), provided that there is some mechanism to feed the internal engine activity for extended time periods. Although Type I collapsar models with prompt black hole formation cannot explain late-time internal engine activity (MacFadyen et al. 2001), the fallback of material onto the central black hole after a stellar collapse could last for long time periods (Woosley 1993; MacFadyen et al. 2001) and lead to late internal engine activity, albeit with significantly reduced luminosity. Continued energy release due to dynamics of a magnetized disk around a black hole, as described by Katz (1997), and/or continued and sporadic emission due to fragmentation and subsequent accretion during the collapse of a rapidly rotating stellar core, as described by King et al. (2005), could both explain observations of extended production of internal shocks. Continued and sporadic internal engine activity has also been explained by Perna et al. (2006) as an effect resulting from large-amplitude gravitational instabilities in the outer accretion disk.

In the time period since the analysis of the data from this GRB, *Swift* has detected several more GRBs with X-ray flares (Nousek et al. 2005). In the near future, it will be possible to use samples of many GRBs with X-ray flares to test models of long-timescale prompt emission.

This work is supported at Penn State by NASA contract NAS5-00136, at the University of Leicester by the Particle Physics and Astronomy Research Council under grant PPA/Z/S/2003/00507, and at Brera Astronomical Observatory by funding from ASI under grant I/R/039/04.

REFERENCES

Band, D., et al. 1993, ApJ, 413, 281
Barthelmy, S., et al. 2004, Proc. SPIE, 5165, 175
Bloom, J. S., Frail, D. A., & Kulkarni, S. R. 2003, ApJ, 594, 674
Burrows, D. N., et al. 2005a, Space Sci. Rev., 120, 165
———. 2005b, Science, 309, 1833
Cash, W. 1979, ApJ, 228, 939
Cenko, S. B., et al. 2005, GCN Circ. 3358, http://gcn.gsfc.nasa.gov/gcn/gcn3/3358.gcn3
Connaughton, V. 2002, ApJ, 567, 1028
Cummings, J., et al. 2005, GCN Circ. 3339, http://gcn.gsfc.nasa.gov/gcn/gcn3/3339.gcn3
Dickey, J. M., & Lockman, F. J. 1990, ARA&A, 28, 215
Falcone, A., et al. 2005, GCN Circ. 3330, http://gcn.gsfc.nasa.gov/gcn/gcn3/3330.gcn3
Frontera, F., et al. 2004, ApJ, 614, 301
Galli, A., & Piro, L. 2005, A&A, submitted (astro-ph/0510852)
Gehrels, N., et al. 2004, ApJ, 611, 1005
Ghirlanda, G., Ghisellini, G., Firmani, C., Celotti, A., & Bosnjak, Z. 2005, MNRAS, 360, L45
Ghisellini, G., Celotti, A., & Lazzati, D. 2000, MNRAS, 313, L1
in't Zand, J. J. M., et al. 2003, in ASP Conf. Ser. 312, Third Rome Workshop on Gamma-Ray Bursts in the Afterglow Era, ed. M. Feroci et al. (San Francisco: ASP), 18
Ioka, K., Kobayashi, S., & Zhang, B. 2005, ApJ, 631, 429
Katz, J. I. 1997, ApJ, 490, 633
King, A., et al. 2005, ApJ, 630, L113
Kobayashi, S., Zhang, B., Mészáros, P., & Burrows, D. 2005, ApJ, submitted (astro-ph/0506157)
Lazzati, D., & Perna, R. 2002, MNRAS, 330, 383
———. 2003, MNRAS, 340, 694
MacFadyen, A. I., Woosley, S. E., & Heger, A. 2001, ApJ, 550, 410
Meegan, C. A., et al. 1996, ApJS, 106, 65
Mészáros, P. 2002, ARA&A, 40, 137
Mészáros, P., & Rees, M. J. 1997, ApJ, 476, 232
Morrison, R., & McCammon, D. 1983, ApJ, 270, 119
Nousek, J. A., & Shue, D. R. 1989, ApJ, 342, 1207
Nousek, J. A., et al. 2006, ApJ, in press (astro-ph/0508332)
Pagani, C., et al. 2005, GCN Circ. 3333, http://gcn.gsfc.nasa.gov/gcn/gcn3/3333.gcn3
Perna, R., Armitage, P. J., & Zhang, B. 2006, ApJ, 636, L29
Piran, T. 2005, Rev. Mod. Phys., 76, 1143
Piro, L., et al. 2005, ApJ, 623, 314
Rhoads, J. E. 1999, ApJ, 525, 737
Romano, P., et al. 2006, A&A, in press (astro-ph/0601173)
Roming, P., et al. 2005, Space Sci. Rev., 120, 95
van Paradijs, J., Kouveliotou, C., & Wijers, R. A. M. J. 2000, ARA&A, 38, 379
Watson, D., Reeves, J. N., Hjorth, J., Jakobsson, P., & Pederson, K. 2003, ApJ, 595, L29
Woosley, S. E. 1993, ApJ, 405, 273
Zhang, B., & Mészáros, P. 2004, Int. J. Mod. Phys. A, 19, 2385
Zhang, B., et al. 2006, ApJ, in press (astro-ph/0508321)